INSTITUTE OF PHYSICS PUBLISHING and INTERNATIONAL ATOMIC ENERGY AGENCY NUCLEAR FUSION

Nucl. Fusion **45** (2005) 226–237 doi:10.1088/0029-5515/45/4/002

Beam anisotropy effect on Alfvén eigenmode stability in ITER-like plasmas

N.N. Gorelenkov[1], **H.L. Berk**[2] **and R.V. Budny**[1]

[1] Princeton Plasma Physics Laboratory, PO Box 451, Princeton, NJ 08543-0451, USA
[2] Institute for Fusion Studies, The University of Texas, Austin, Texas 78712, USA

Received 16 August 2004, accepted for publication 8 February 2005
Published 16 March 2005
Online at stacks.iop.org/NF/45/226

Abstract
This work studies the stability of the toroidicity-induced Alfvén eigenmodes (TAE) in the proposed ITER burning plasma experiment, which can be driven unstable by two groups of energetic particles, the 3.5 MeV α-particle fusion products and the tangentially injected 1 MeV beam ions. Both species are super-Alfvénic but they have different pitch angle distributions and the drive for the same pressure gradients is typically stronger from co-injected beam ions as compared with the isotropically distributed α-particles. This study includes the effect of anisotropy of the beam ion distribution function on TAE growth rate directly via the additional velocity space drive and indirectly in terms of the enhanced effect of the resonant particle phase space density. For near parallel injection TAEs are marginally unstable if the injection aims at the plasma centre, where the ion Landau damping is strong, whereas with the off-axis neutral beam injection the instability is stronger with the growth rate near 0.5% of the TAE mode frequency. In contrast, for perpendicular beam injection TAEs are predicted to be stabilized in nominal ITER discharges.

In addition, the effect of TAEs on the fast ion beta profiles is evaluated by introducing a fast ion redistribution toy model based on a quasi-linear diffusion theory, which uses analytic expressions for the local growth and damping rates. These results illustrate the parameter window that is available for plasma burn when TAE modes are excited.

PACS numbers: 52.35.Bj, 52.55.Pi.

(Some figures in this article are in colour only in the electronic version)

1. Introduction

The toroidal Alfvén eigenmodes (TAEs) [1–4] destabilized by fast ions can cause significant difficulties for the containment of energetic alpha particles in fusion energy generating tokamak experiments. Experimentally, it is also known that various conditions can be obtained with varying degrees of severity. The modes can be stable, or unstable where energetic particle loss is insignificant [5, 6]. However, it was established that in the presence of a strong enough energetic particle energy density these modes will induce large losses of fast particles.

In the proposed ITER fusion experiment, 1 MeV neutral beam injection (NBI) is planned for current drive and auxiliary heating [7]. The neutral beams will be injected in the direction of the plasma current and will create an anisotropic distribution of super-Alfvénic beam ions, which will drive TAEs unstable with partial growth rate contributions that are comparable to the contribution from fusion alphas [8]. In this reference, it was found that for a nominal ITER experiment operating with the central temperature at 20 keV, the plasma would be marginally unstable to alpha particle TAE instability. An initial study of the beam ion contribution to the TAE drive showed that the beams were an additive contribution to the alpha particle instability. In addition, it was shown that the anisotropy in the beam ion distribution function results in an additional velocity space drive. Since the beam ion contribution is significant it is important to carefully evaluate this mechanism and, if possible, find a TAE stable plasma parameter domain.

The purpose of the first part of this paper is to determine the effect of beam ions with an anisotropic distribution function on the linear instability of TAEs under burning plasma conditions. We use the perturbative NOVA/NOVA-K codes [9, 10], which were successfully employed to predict the thresholds and frequencies of medium-n TAE instabilities in various experiments including the beam heated deuterium–tritium experiments on TFTR [11, 12]. Recently, NOVA/NOVA-K codes were successfully used to explain high-n odd core localized TAEs observed in ICRH JET discharges [13]. In these codes the procedure used is to first obtain the lowest order mode structure using the ideal MHD NOVA code, which neglects damping and drive sources. Then, the NOVA-K code incorporates these sources through a perturbative procedure by evaluating the corresponding integrals over the known eigenfunctions. At moderate- to high-n the lowest order

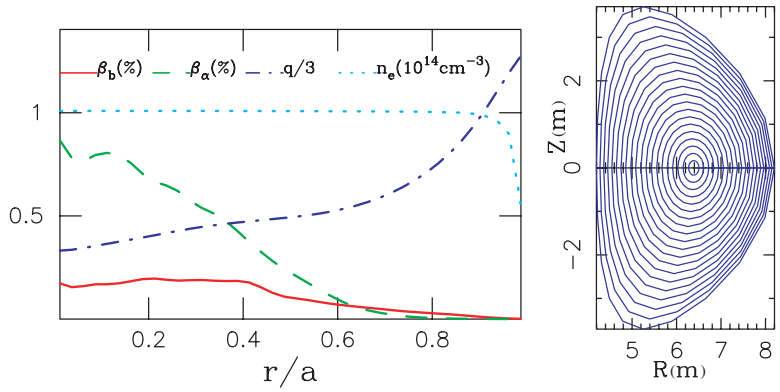

Figure 1. Plasma profiles for the ITER plasma equilibrium (left plot) and corresponding magnetic surfaces (right plot) as predicted by the TRANSP code. On the left plot are shown the beam beta β_b (%), the fusion alphas beta β_α (%), safety factor q and the electron density n_e (10^{14} cm^{-3}).

TAE mode often extends over the entire minor radius. When the continuum is not excited in the regions where the amplitude of the eigenmode is significant, the global structure of the TAE mode can then be used as a lowest order approximation to the eigenmode. Then, the beam ion drive and other numerous damping mechanisms are incorporated in a perturbative manner to predict stability. All equilibrium plasma parameters and profiles are obtained by employing the transport code TRANSP [14]. In this paper, we analyse details of TAE stability for one of the most unstable toroidal mode numbers, $n = 10$, to examine the sensitivity to NBI injection characteristics, such as geometry and energy.

One can expect TAE unstable plasmas to still produce tolerable reactor performance if only moderate alpha transport is induced, which primarily redistributes the alpha particle profile inside the plasma rather than causing direct losses to the plasma facing walls. The strength of the redistribution should depend upon how far above the marginal threshold the modes are excited, among other factors. We propose a model in section 6 in which the local TAE stability theory is applied to reconstruct the self-consistent fusion alphas beta profiles on the basis of a quasi-linear diffusion model. This model makes use of expressions for the local growth and damping rates and calculates the relaxed alpha particle profiles by imposing the particle conservation condition for the steady state.

2. ITER plasma modelling

Equilibrium plasma profiles of the ITER nominal discharge are calculated by the transport code TRANSP [14] and are presented in figure 1, where the plasma density, safety factor, alpha particle and beam ion beta profiles are plotted as functions of the minor radius variable $r/a \equiv \sqrt{\Phi}$, where Φ is the toroidal magnetic field flux, normalized to 1 at the plasma edge and 0 at the plasma centre. Other plasma parameters we use are: a major plasma radius of the geometrical centre of $R_0 = 6.2$ m, a minor radius of the last magnetic surface of $a = 2$ m, a deuterium negative NBI injection power $P_{\rm NBI} = 33$ MW at an energy $E_{b0} = 1$ MeV, a vacuum magnetic field at the geometrical axis of $B_0 = 5$ T, a total central beta value of $\beta_0 = 6.7\%$ and ion and electron temperatures in the centre at $T_{i0} = 19.5$ keV and $T_{e0} = 23.5$ keV, respectively.

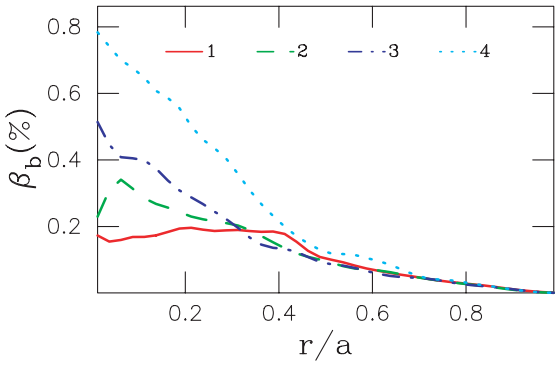

Figure 2. Equilibrium beam beta profiles in four ITER plasmas under consideration. Curves 1, 2 and 3 are for the plasma ion temperature $T_{i0} = 19.5$ keV, and injection geometry aiming with vertical shifts of 0.55 m, 0.35 m and 0 m, respectively, with respect to the equatorial plane. Curve 4 corresponds to the on-axis NBI at plasma temperature $T_{i0} = 25.3$ keV.

The injection geometry is taken from the latest ITER design[3] and is slightly different from the one used in earlier calculations [8, 14], which results in up to approximately 50% lower fast ion beta values. These parameters were input to TRANSP simulations where NBI was applied tangentially 0.55 m below the magnetic axis. Note that the resulting safety factor profile has a region of lower shear at $r/a \sim 0.5$ because the proposed NBI and ICRH modify the current density profile. The low shear region turns out to be important for the stability considerations of global TAEs.

This set of plasma parameters corresponds to one of the most unstable cases we have considered. In this case, the beam injection produces a hollow beam beta profile and a strong pressure gradient in the region $r/a \sim 0.5$, which is the region where the damping is relatively weak, which allows TAEs to be excited (more details are given below).

In addition to case (1) with 0.55 m off-axis NBI, three other injection configurations have been studied (cases (2), (3) and (4)) as shown in figure 2. In all these cases the plasma beta was fixed at a beta value that is characteristic of the value expected by the constraint that the discharge be MHD stable. Cases (2) and (3) are for fixed $T_{i0} = 19.5$ keV, with case (2)

[3] http://www.iter.org/

with on-axis injection while case (3) is for 0.35 m off-axis. The third additional case is for a higher ion temperature, $T_{i0} = 25.3$ keV and on-axis NBI.

2.1. NBI ion anisotropic distribution function

Since the beam injection creates an anisotropic beam ion distribution function, one needs to model it carefully due to its potentially strong effect on TAE stability. In this study, we develop a model for the co-injected (as proposed for the ITER design) beam ion slowing down distribution function and a Gaussian in pitch angle dependence, centred at some average value, χ_0, where $\chi \equiv v_\parallel/v$ is the pitch angle taken at the equatorial plane at the low field side of the plasma cross section. We will see that this model captures the main physics relevant for AE stability analysis and which appears to be consistent with the results obtained from the Monte Carlo post-processor of the TRANSP code [14].

As we take the ions to be injected in the passing region parallel to the current flow, $\chi_0 > 0$, the trapped and the passing particles that flow in the direction opposite to the plasma current only appear in the plasma due to Coulomb collisional scattering. Special care is then needed in accounting for such particles in the distributions we study. To high accuracy this distribution function obeys the steady solution in terms of the integrals of motion (IOM) of the drift kinetic equation (see, e.g. [15]). The selection of the equation needs special consideration to be compatible with the collisional slowing down process. In general, this problem needs to be solved numerically, which is a difficult and beyond the scope of this paper. Instead, we select a distribution function form that qualitatively captures the effect of collisions. First, superthermal fast ions slow down on electrons and ions, which is consistent with the following form of the distribution function, $f_b = \hat{f}/(v^3 + v_*^3)$, where v_* is the critical velocity at which the ion collisional drag becomes comparable with the drag on electrons. The problem of finding $\hat{f}$ can be reduced to the following equation:

$$\frac{\partial \hat{f}}{\partial \tau} = \frac{\partial}{\partial \chi} d_{\chi\chi} \frac{\partial \hat{f}}{\partial \chi} + Q\delta(\chi - \chi_0)\theta(\tau - \tau_0), \qquad (1)$$

where $\mathrm{d}\tau \equiv \mathrm{d}v v_*^3/v(v^3 + v_*^3)$ or $\tau = -\frac{1}{3}\ln[(1 + v_*^3/v_{b0}^3)/(1 + v_*^3/v^3)]$, v_{b0} is the injection velocity (at $\tau = \tau_0$), θ the step function, τ_{se} the ion slowing down time due to collisions with electrons, Q the beam ion source and $\tau_0 = \tau_{|v=v_0}$. Here, we assumed that the injection is at a single pitch angle χ_0 and implied that the pitch angle scattering coefficient is $D_{\chi\chi} = v_*^3 d_{\chi\chi}/v^3\tau_{se}$. First, we consider the case with the constant diffusion coefficient, $d_{\chi\chi} = 1$, which allows for the analytical solution in the homogeneous plasma. For narrow pitch angle distributions, this solution of equation (1) has Gaussian dependence:

$$\hat{f} = f_\chi(\chi, v, r)C(r), \qquad \text{if } v < v_{b0} \qquad (2)$$

and $\hat{f} = 0$ if $v > v_{b0}$, where $f_\chi(\chi, v, r) \equiv \mathrm{e}^{-(\chi-\chi_0)^2/\delta\chi(v,r)^2}/\delta\chi(v, r)\sqrt{\pi}$, and $\delta\chi^2 \ll \chi_0^2$ is assumed. In this formula $\delta\chi$ is the width of the pitch angle distribution function, $C(r)$ is the normalization function. Note that f_b is a function of a particle's IOM, since χ at the low field side can be expressed in terms of IOM. The pitch angle width $\delta\chi(v, r)$ changes as fast ions slow down due to the Coulomb scattering [16,17]. The form of $\delta\chi(v, r)$ can be straightforwardly derived by noting that while beam ions slow down they experience Coulomb scattering. Simultaneously, the particle velocity is determined from the velocity drag and it is found to satisfy

$$v^3 = (v_*^3 + v_{b0}^3)\,\mathrm{e}^{-(3t/\tau_{se})} - v_*^3. \qquad (3)$$

At a given time, the pitch angle width is broadened according to equation $\delta\chi^2 = \delta\chi_0^2 + \int_0^t D_{xx}\,\mathrm{d}t$, where $\delta\chi_0$ is the initial width due to ion finite orbit width (FOW) and plasma aspect ratio effects. Thus, it follows that the width is given by

$$\delta\chi^2(v, r) = \delta\chi_0^2 - \frac{1}{3}\ln\left[\frac{v^3(1 + v_*^3/v_{b0}^3)}{v^3 + v_*^3}\right]. \qquad (4)$$

The centre of the pitch angle Gaussian distribution function, χ_0, is computed by taking the first moment of the numerical distribution function generated by TRANSP. In the case analysed, we obtained $\chi_0 \simeq 0.8$ near the region of interest, i.e. $r/a \simeq 0.5$ and χ_0 does not change significantly in the vicinity of the TAE location.

Figure 3(*a*) shows contours of constant f for the distribution function generated by TRANSP and the numerical pitch angle distribution widths $\delta\chi^2$, are shown in figure 3(*b*) along with the widths fitted to the analytic results,

$$\delta\chi^2(v, r) = \delta\chi^2(v) = 0.015 - \frac{1}{3}\ln\left[\frac{(v/v_{b0})^3 1.275}{(v/v_{b0})^3 + 0.275}\right]. \qquad (5)$$

In making a fit to the numerical width we used velocity parametric dependence whereas other coefficients were computed. Here, the minor radius dependence can be neglected within the mode location. Equation (5) implies that $v_*^2/v_{b0}^2 = 0.423$, which is the typical predicted value for ITER.

If the pitch angle width becomes large, the above χ dependence of the distribution function needs to be modified. Consider three regions: (I) positive passing ions $\chi_{s+} < \chi < 1$, where χ_{s+} is the pitch angle at the separatrix between the co-moving (with respect to the plasma current) passing and the trapped ones; (II) trapped ions $\chi_{s-} < \chi < \chi_{s+}$ and (III) negative passing ions $-1 < \chi < \chi_{s-}$, where χ_{s-} refers to the separatrix between the counter-moving passing and trapped ions. In the case of a large aspect ratio plasma $\chi_{s+} = -\chi_{s-} = \sqrt{2\epsilon}$. If we relax the boundary condition at $\chi = -1$ we can then satisfy the boundary condition for the particle flux near the separatrix by the method of images. The flux condition requires that the fluxes in and out of the separatrix region are equal:

$$\frac{\partial f(\chi_{s+} + \delta)}{\partial \chi}\tau_+ = \frac{\partial f(\chi_{s-} - \delta)}{\partial \chi}\tau_- + \frac{\partial f(\chi_{s+} - \delta)}{\partial \chi}\tau_+ + \frac{\partial f(\chi_{s-} + \delta)}{\partial \chi}\tau_-,$$

where τ_+ is the part of trapped particle drift orbit period containing particle positive parallel velocity, τ_- corresponds to the rest of the particle orbit and δ is an infinitesimal small number. In the above condition for fluxes we also assumed that the separatrix dependence on velocity is weak. In the following, we present the derivation for the case of large aspect ratio plasmas without fast ion orbit effects, in which

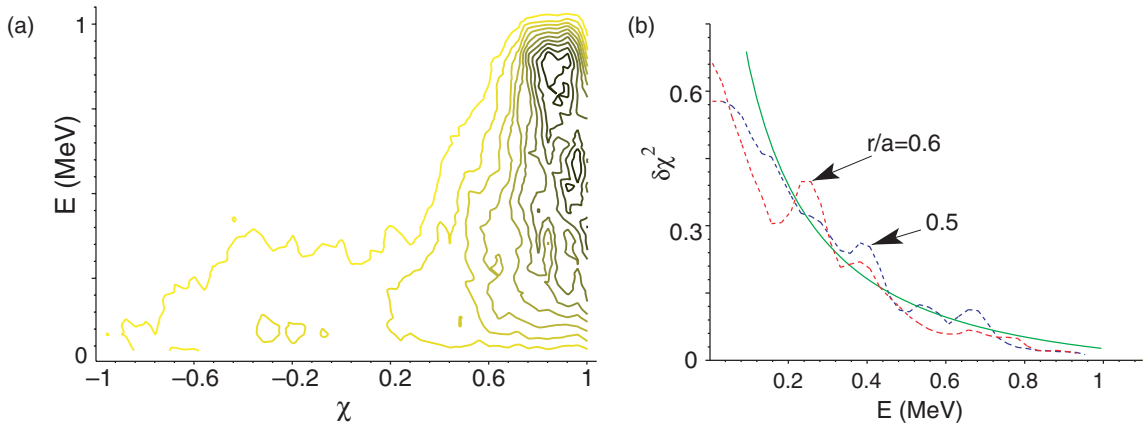

Figure 3. Contours of constant distribution function of beam ions (*a*) taken at the low field side of the plasma cross section and averaged over $0.5 < r/a < 0.6$. (*b*) Shows the pitch angle width of the beam ion distribution function versus particle energy at two minor radii $r/a = 0.5$ and 0.6. These plots compare favourably with the widths resulting from the analytic model (- - - -) given by equation (5).

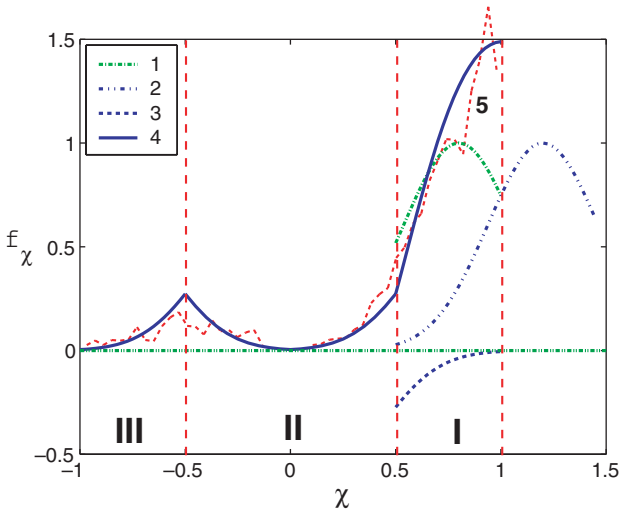

Figure 4. Results of modelling the beam ion pitch angle distribution function as given by equation (7) (curve 4) and its comparison with the TRANSP simulation (curve 5). The different pitch angle regions correspond to (I), co-passing beam ions; (II), trapped ions; and (III), counter-passing ions. In this case, we used the low aspect ratio approximation for parameters $\delta\chi = 0.37$ and $r/R = 1/8$. Also shown are different terms for the model distribution function in region I: curves 1 and 2 correspond to first and second terms on the right-hand side of equation (6), whereas curve 3 is the sink term (second term of equation (7) for region I).

$\tau_- = \tau_+$, the flux condition equation reads $f'(\chi_{s+} + \delta) = f'(\chi_{s-} - \delta) + 2f'(\chi_{s+} - \delta)$, and we require that the trapped ion distribution function inside the region II is even in χ.

Since the possible pitch angle range is bounded by $|\chi| < 1$, image particle sources can be introduced in order not to have diffusive fluxes at the boundaries. In that case the distribution function satisfies the physical requirement of zero derivative at the boundary

$$f_{\chi p}(\chi) = \phi(\chi) \equiv \frac{\mathrm{e}^{-(\chi-\chi_0)^2/\delta\chi^2} + \mathrm{e}^{-(\chi-2+\chi_0)^2/\delta\chi^2}}{\delta\chi\sqrt{\pi}}, \qquad (6)$$

where the two terms on the right-hand side correspond to curves 1 and 2 shown in figure 4. Since particles are diffusing out of the region I an image sink needs to be introduced. In regions II and III image sources at half the actual source strength adequately represent the solution. Thus, we finally obtain

$$f_\chi = \begin{cases} \phi(\chi) - \frac{1}{2}\phi(2\chi_{s+} - \chi), & \text{region I,} \\ \frac{1}{2}\phi(-\chi) + \frac{1}{2}\phi(\chi), & \text{II,} \\ \frac{1}{2}\phi(2\chi_{s+} + \chi), & \text{III.} \end{cases} \qquad (7)$$

The procedure described is valid for a broad range of pitch angle widths and the truncation only becomes invalid at late times when it is necessary to account for collisional fluxes resulting from multiple reflections from the confinement boundaries. In this case, one can in principle add an infinite series of images (or solve equation (1), with the correct boundary conditions, numerically or analytically using a Fourier representation) to obtain a more isotropic-like solution. In our analysis, such an addition is not required because fast ions at energies such that $\delta\chi \sim 1$, are typically out of resonance with TAEs, a result that is confirmed by numerical analysis. For negative χ_0, the model is essentially the same as what has been described, whereas for the case of perpendicular injection, i.e. $\chi_0 < \chi_s$ the distribution function can be constructed as $f_\chi = [\phi(\chi) + \phi(-\chi)]/2$ for all χ regions.

The normalization function $C(r)$ in equation (2) is calculated by taking the radial profile of beam ion beta from the TRANSP analysis code and integrating $v^2 f_\mathrm{b}/2$ over the velocity space to construct the local value of beta, $\beta_\mathrm{b}(r)$. We find $\beta_\mathrm{b}(r) = (2^3\pi m_\mathrm{b}/3B_0^2)\int v^2 f_\mathrm{b}\,\mathrm{d}^3v$, which implies

$$C(r) = \frac{3B_0^2\beta_\mathrm{b}(r)}{2^5\pi^2 E_{\mathrm{b}0}}\left\{\frac{1}{2} + \frac{v_*^2}{6v_{\mathrm{b}0}^2}\ln\left[\frac{(v_{\mathrm{b}0}+v_*)^3}{v_{\mathrm{b}0}^3+v_*^3}\right] + \frac{v_*^2}{\sqrt{3}v_{\mathrm{b}0}^2}\arctan\left[\frac{v_*-2v_{\mathrm{b}0}}{\sqrt{3}v_*}\right] - \frac{\sqrt{3}\pi v_*^2}{18v_{\mathrm{b}0}^2}\right\}^{-1}. \qquad (8)$$

The above calculations were performed to lowest order aspect ratio where toroidicity effects are ignored. As we show, this result is compatible locally with the one obtained by TRANSP in the equatorial plane, $\theta = 0$. We expect that this result is also compatible with the TRANSP beam beta radial profiles, which is an average over the poloidal angle. This is because the NBI is close to tangential and the beam ion drift orbit radial width is small.

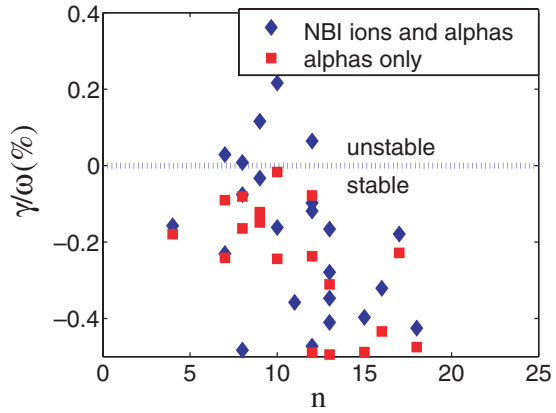

Figure 5. Toroidal mode number dependence of the TAE growth rates for the cases with the drive from alpha particles only (■), and with the drive from both NBI ions and alpha particles (♦).

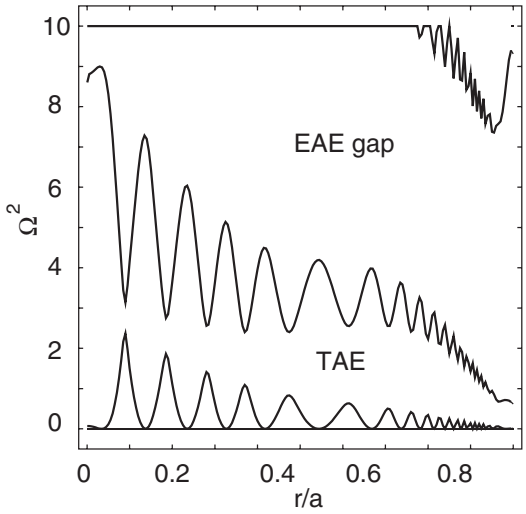

Figure 6. Alfvén continuum with gaps due to toroidal (TAE gap) and poloidal (EAE gap) coupling for $n = 10$ as calculated by the NOVA code.

Finally, we present the case with more realistic Lorentz collisional pitch angle scattering coefficient in appendix A. Both forms of the distribution function give very similar results for the growth rates for TAEs in ITER. This is because they have the same narrow anisotropic pitch angle distribution at high beam ion velocities, where ions resonate with TAEs, whereas the collisional scattering happens at lower velocities and with different scattering coefficients.

3. TAE stability analysis

3.1. NOVA eigenmode analysis

In a previous numerical study [8] the domain of the most unstable TAE toroidal mode numbers ($n = 7$–20) in a nominal ITER plasma was computed using the global hybrid kinetic code NOVA-K. In this paper, the fast ion beta estimate is somewhat lower than that used in [8] due to both a change in the injection geometry and the use of a better NBI confinement model in the TRANSP code. Hence, as the near-threshold stability analysis is sensitive to the fast ion beta we repeat the toroidal mode number scan similar to the one presented earlier. The results are shown in figure 5 for the nominal ITER plasma with on-axis NBI. We observe that due to the lower beam and alphas' beta values the range of unstable n-values only spans from 7 to 12 for the case when both alpha particle and beam ion drives are included. It can be seen that TAEs are near threshold, and alpha particles alone do not seem to be sufficient to destabilize TAEs. As a measure of how close we are to marginal stability we note that from table 1 (to be discussed later) one can see that the growth rate from alphas and beams for $n = 10$ is $\sim$1.5% of the eigenmode frequency, compared to $\sim$0.3% for the predicted growth rate when damping is accounted for.

In this section we analyse in detail the TAE stability for one of the most unstable toroidal numbers, $n = 10$, in order to examine the sensitivity of the NBI drive to the injection characteristics, such as geometry and energy. The toroidicity and ellipticity induced gaps in the Alfvén continuum are calculated and are shown in figure 6 for the nominal ITER plasma discharge with 0.55 m off-axis NBI [7, 14]. The normalized frequency is $\Omega = \omega q_1 R_0/v_{A0}$, where v_{A0} is the central Alfvén velocity, q_1 is the edge value of the safety factor and R_0 is the major radius of the geometrical centre. The centre of the TAE gap envelope is proportional to the dependence $1/q\sqrt{n_e}$, so that in tokamaks, often, the gap is nearly aligned along the minor radius, thereby allowing the TAE mode to span along a large portion of the minor radius without strongly interacting with the continuum. This was observed in present-day experiments, where a more open gap corresponds to MHD activity in the TAE frequency range (see, e.g. [18–20]), whereas the plasma with the closed gap did not show such activity. The TAE gap in figure 6 is aligned except at the very edge due to strong variation of the safety factor towards the edge and flat density profile. This may result in TAE damping for global low-n modes. In this work, the continuum damping is not included.

The NOVA-K hybrid code predicts $n = 10$ TAEs to be unstable in this ITER example if both the alpha particle, γ_α, and beam ion, γ_{beam}, drives are combined. Among the various damping mechanisms that significantly reduce the drive are ion Landau damping, γ_{iLand}, radiative damping, γ_{rad} and trapped electron collisional damping, γ_{ecoll}. The sum of damping and drive terms is plotted in figure 7 versus what we call the NBI impact parameter, ΔZ_{NBI}, which is the vertical deviation from the magnetic axis of the beam injection line. For each case, up to two eigenmodes are unstable. The more the beam is directed off-axis the stronger the drive is. This is because during the on-axis NBI, beam ion beta builds up near the plasma centre (see figure 2), where the ion Landau damping is very strong. With the off-axis NBI the region of the strong beta gradient is shifted outwards to the middle of the minor radius (e.g. 0.55 m off-axis, figure 2), so that both central ion Landau damping and edge trapped electron collisional damping are decreased. For the higher ion temperature case, $T_{i0} = 25.3$ keV, the fusion beta is larger, which enhances alpha particle destabilization of the TAE instability. However, even in that case, where $\beta_{\alpha 0} \simeq 1.33\%$, the pure fusion alpha-particle instability seems still to be marginally stable for $n = 10$. However, with NBI present, the instability drive is strong enough to cause instability, with the growth rates for the most

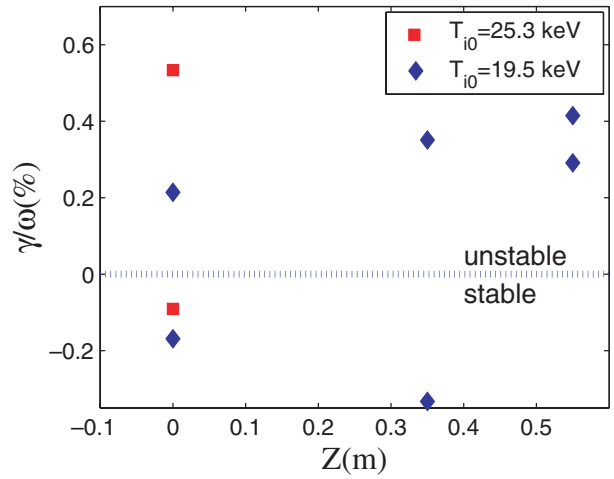

Figure 7. The $n = 10$ unstable TAE growth rates determined as functions of the NBI impact parameter (vertical deviation from the magnetic axis).

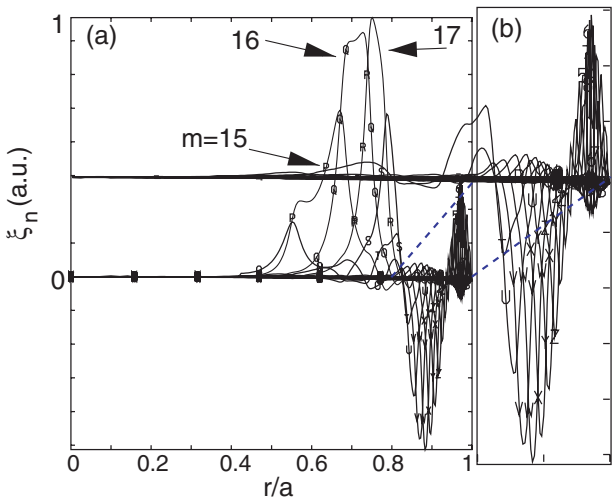

Figure 8. Radial mode structures of poloidal harmonics of the radial plasma displacement (a) for one representative TAE mode with $\Omega^2 = 0.96$ in the case of 0.55 m off-axis NBI. (b) Shows zoomed eigenmode poloidal harmonics at the edge without singularities on their structure, which indicates that the edge continuum damping is expected to be small.

unstable mode at $\gamma_\Sigma/\omega = 0.55\%$. The contribution to the drive from alphas or beam ions is typically ∼1–3%, which is, with damping included, probably sufficiently small for the perturbation approach to be adequate.

As an example, we present the stability properties of one of the most unstable $n = 10$ TAEs for 0.55 m off-axis NBI. The radial structure of poloidal harmonics of this mode is presented in figure 8 versus the minor radius, which is defined as $r/a \equiv \sqrt{\psi/\psi_0}$, where ψ is the poloidal magnetic flux, ψ_0 the flux at the plasma edge, and we assumed $\psi = 0$ at the magnetic axis. Comparing figures 6 and 8, one can see that the mode is located in the gap with only a weak interaction with the continuum on the left. At that point its amplitude is small, which means that continuum damping is expected to be small [21, 22]. As the output of the TRANSP code shows, because of the neutral beam current drive, there is a low shear region at $0.4 < r/a < 0.6$ near the mode resonance with the Alfvén continuum, where $s < 0.3$. This implies that the 'propagation' of TAE 'couplets' into the centre can be weak, with the result of low continuum damping $\gamma/\omega < 0.001$ [22]. The mode structure at the edge is zoomed in on figure 8(b) and does not show TAE interaction with the continuum. We also note that in the $n = 1$ TAE, strong damping was observed experimentally as the safety factor shear increases at the edge [23], which can indicate strong continuum damping of that mode. However, more recent results of externally excited $n \sim 4$ TAEs [24] do not show such correlation, which suggests that as expected high-n modes are less global and weakly interact with the continuum at the edge.

Table 1. Damping and driving growth rates of one of the most unstable $n = 10$ TAE in the case of 0.55 m off-axis NBI. The TAE normalized eigenfrequency is also given.

Ω^2	$\gamma_{\rm ecoll}/\omega$ (%)	$\gamma_{\rm iLand}/\omega$ (%)	$\gamma_{\rm rad}/\omega$ (%)	γ_α/ω (%)	$\gamma_{\rm beam}/\omega$ (%)	γ_Σ/ω (%)
0.96	−0.18	−0.61	−0.43	0.82	0.71	0.31

Table 1 lists the calculated damping mechanisms and drive terms due to alpha particles and beam ions at $\mathcal{E}_{\rm b0} = 1$ MeV. Though the beams are at lower beta value than the alpha particles, their drive is comparable due to their anisotropy at a fixed energetic particle energy density, as is discussed in the next section. Note that the three damping mechanisms are equally important for TAE stability, whereas, as the calculations show at high n ($n > 15$), the radiative damping becomes dominant and stabilizes the modes.

4. Theory of NBI anisotropy effect on TAEs

The anisotropy effect on the TAE drive has been studied for fast ions with beam-like anisotropic distributions [25] and for fusion products such as alphas with natural anisotropy due to FOW effects [26, 27]. For simplicity let us present the calculation of the drive in the case of the beam ion anisotropic distribution, where there is a delta function pitch angle dependence of the form

$$f_{\rm b} \simeq \frac{3\beta_{\rm b}B^2}{2^4\pi^2 E_{\rm b0} v^3}\theta(v_{\rm b0} - v)\delta(\chi - \chi_0), \qquad (9)$$

where θ is the step function. Note, that in the approximation of strongly passing beam ions (i.e. $\chi_0 \sim 1$, which is reasonable for the tangential beam injection in ITER) χ does not change along the particles's drift trajectory. For simplicity, we take a zero orbit radial width for the beam ion trajectories. Then, the growth rate for the shear Alfvén instability reads [28]

$$\frac{\gamma}{\omega} \simeq -\frac{v_{\rm A}^2 m_{\rm b}^2 \pi^2}{2\omega R^2 B^2 E_{\rm b0}} \int {\rm d}^3 v \left[-\frac{E_{\rm b0}\partial}{\partial E} - \frac{\omega_*}{\omega}\right] f_{\rm b} \left(\frac{v_\perp^2}{2} + v_\parallel^2\right)^2 \times \delta\left(\omega - \left(k_\parallel \pm \frac{1}{qR}\right) v_\parallel\right),$$

where ω_* is the diamagnetic frequency of beam ions. This can be integrated directly and the expression for the growth rate reads

$$\frac{\gamma}{\omega} \simeq \frac{-3\pi\beta_{\rm b} q^2}{8} \frac{v_{\rm A}^2}{v_{\rm b0}^2} \frac{(1+\chi_0^2)^2}{\chi_0^2}\left[3 + \frac{\chi_0^2}{(1+\chi_0^2)^2}\frac{\partial}{\partial\chi_0} \times \left(\frac{(1-\chi_0^2)(1+\chi_0^2)^2}{\chi_0^3}\right) - \frac{2v_{\rm A}^2}{v_{\rm b0}^2}\frac{\omega_*}{\chi_0^2\omega}\right],$$

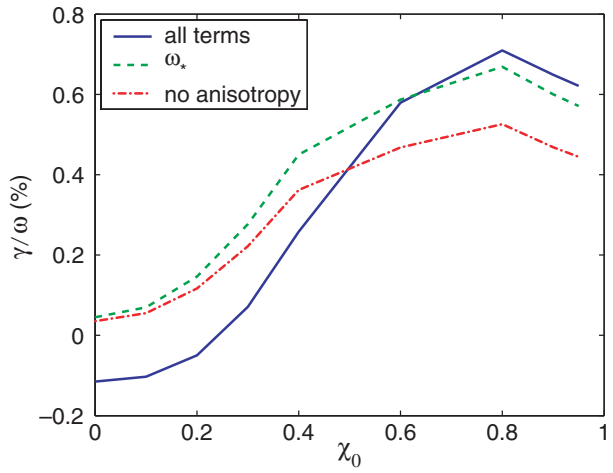

Figure 9. Pitch angle, χ_0 (at fixed $\delta\chi^2 = 0.05$) dependence of different driving terms in the TAE growth rate. The solid curve is for all the driving terms, whereas the dashed curve is for velocity plus spatial gradient terms and the dot–dashed curve is for the spatial gradient term alone.

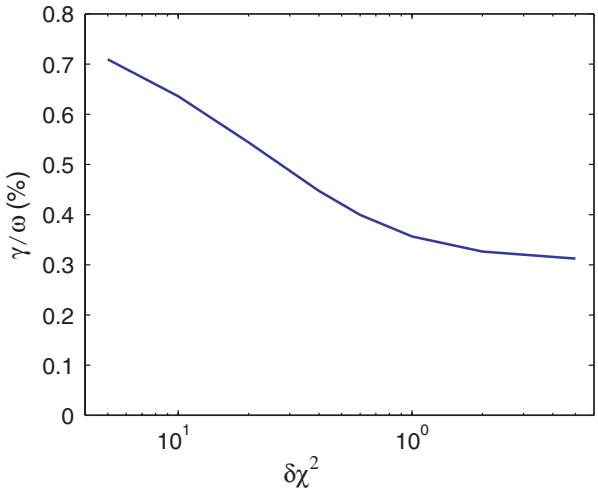

Figure 10. The growth rate dependence versus the beam ion distribution parameter $\delta\chi^2$ taken for $\chi_0 = 0.8$.

which can be transformed to

$$\frac{\gamma}{\omega} \simeq \frac{-3\pi\beta_b q^2}{8}\frac{v_A^2}{v_{b0}^2}\frac{(1+\chi_0^2)^2}{\chi_0^2} \times\left[3-\frac{(3-2\chi_0^2+3\chi_0^4)}{\chi_0^2(1+\chi_0^2)}-\frac{2v_A^2}{v_{b0}^2}\frac{\omega_*}{\chi_0^2\omega}\right]. \quad (10)$$

Appropriate expressions can also be obtained for the case where the beam orbit width is important. In this case, the above results are altered by multiplying equation (10) with a factor Δ_b/Δ_m, where $\Delta_b = q\rho_b$ is the passing beam ion orbit width, ρ_b is the beam ion Larmor radius and $\Delta_m = r_m^2/msR$ is the TAE mode radial width scale [25]. In that case the expression for the growth rate is in a plateau regime with respect to TAE mode number. It follows from equation (10) that the growth rate increases if the injection angle decreases; for example, if χ_0 changes from $\chi_0 = 1$ to a lower value. This is confirmed by the numerical simulations presented in the next section. Note that the additional anisotropy term (second term in equation (10) is destabilizing and it considerably reduces the stabilizing first term. For example, at $\chi_0 = 1$ the sum of the first two terms in the square brackets of equation (10) is smaller than the first term by a factor $\frac{1}{3}$. For $\chi_0 < 1$ the anisotropy term increases faster than the first term in equation (10) so that at $\chi_0 < 0.8$ it becomes larger than the first one.

5. NBI anisotropy effect calculated from NOVA

The properties of the TAE instability drive due to the anisotropic beam ion distribution function are studied with the pitch angle dependence in the form of equation (6) and fixed $\delta\chi^2 = 0.05$ for figure 9 and $\chi_0 = 0.8$ for figure 10. From figure 9 one can see that the drive depends more strongly on the injection pitch angle than on the width of the distribution. Also, calculations show that the drive is stronger for more localized modes. The instability is driven by passing particles rather than by trapped ones for almost all modes. Hence at the perpendicular injection (with $\chi_0 = 0$) TAEs are stable.

The effect of the anisotropy of the beam ion distribution function is also computed by separating each of the driving or damping terms of the growth rate: the ω_* driving term (third term in square bracket of equation (10)), velocity gradient stabilizing term (first term in square bracket of equation (10)) and anisotropy driving term (second term in square bracket of equation (10)). We plot the growth rate as a function of χ_0 including (i) all terms, (ii) spatial gradient drive (ω_* curves) and (iii) velocity plus spatial gradient (no anisotropy curves) as indicated in figure 9. The anisotropy contribution accounts for 30–40% of the drive for tangential injection $\chi_0 \sim 1$. It becomes stabilizing for perpendicular injection, $\chi_0 = 0$. Surprisingly, from figure 9 it follows that the energy derivative alone, i.e. the anisotropy drive plus the velocity drive contribute to the destabilization of the TAE. This seems to contradict the result of equation (10), where the first and second terms in square brackets relate to each other as -3 to 2, so that the net contribution is stabilizing. This is because the distribution function adopted in the derivation of the analytical expression does not include the critical velocity v_*. If it is included, which is the case for the numerical analysis, the velocity and the anisotropy drives are related as follows: $-3v^3/(v^3 + v_*^3)$ to 2. For ITER in which $v_* \sim v_A$ we find that ratio to be ~ -1.5 to 2 so that the energy derivative alone is destabilizing in this case.

Since TAE excitation is due to the particle mode resonance it is expected that the instability will be sensitive to the injection energy. Such an injection energy scan is shown in figure 11. Instability due to the beam ions is stabilized at beam energy $E_{b0} < 200$ keV. Such a low energy may not be enough to achieve the NBI goal of current drive and auxiliary heating because the beam may not penetrate deep enough [8].

6. Relaxation of fast ion profiles in multiple TAE unstable plasma

Finally, we present a toy model for assessing the effect of TAE instabilities on the fast ions. In particular, we attempt to develop a methodology for assessing the case of instability to determine whether or not there is likely to be a substantial loss of energetic particles (and how that depends on plasma

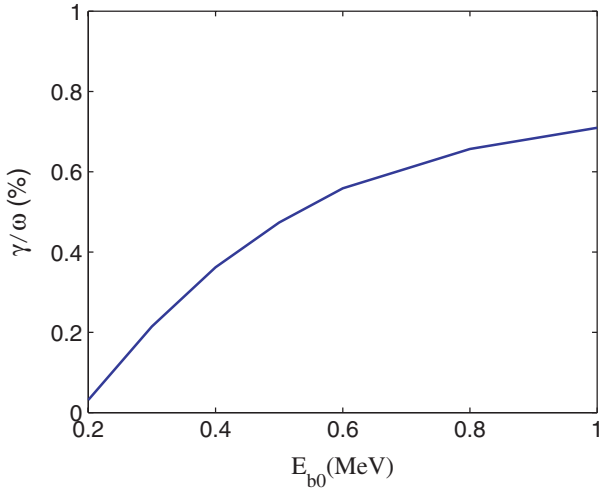

Figure 11. NBI energy dependence of the drive of the $n = 10$ TAE mode.

parameters) due to diffusion from the fields generated by the TAE modes.

In [8] the local critical alpha particle pressure gradient was estimated from the balance between the energetic particle drive and the most probable, important dissipative mechanisms, which were ion Landau damping and trapped electron collisions. Indeed, it was also shown that these two damping mechanisms are dominant for the expected radial location of the most unstable TAEs $r/a \geqslant 0.5$. Equating the drive to damping terms gives,

$$\frac{\partial \beta_{\alpha \mathrm{cr}}}{\partial r} = -\frac{\gamma_{\mathrm{iL}} + \gamma_{\mathrm{ecoll}}}{\gamma'_\alpha}, \tag{11}$$

where $\gamma'_\alpha = \gamma_\alpha/(\partial\beta_\alpha/\partial r)$. Note that the right-hand side of this equation depends on the background plasma parameters and is independent of β_α. In our toy model we consider a one-dimensional quasi-linear equation where the spatially local diffusion coefficient, $D(r)$, grows at a rate proportional to $\gamma_\alpha + \gamma_{\mathrm{iL}} + \gamma_{\mathrm{ecoll}}$. The growth of $D(r)$ causes $-\partial\beta_\alpha/\partial r$ to decrease in the unstable region but the size of the surrounding stable region to increase. The net result is the relaxation of the distribution function to a marginally stable one over a region that is larger than the original instability region. For this model this behaviour is independent of the proportionality constant between the diffusion coefficient and the actual perturbed fields. Consequently, this model makes a prediction for the amount of redistribution and transport of the alpha particles, without performing the complicated calculation of obtaining the perturbed fields that produce the diffusion coefficient.

In the profiles discussed in the previous sections that were based on TRANSP the α equilibrium steady-state beta profile is fitted closely to $\beta_\alpha = 0.008[1 - (r/a)^2]^5$. In this section, we choose this profile for the alphas and the plasma ion temperature profile is taken to be of the form T_{i} (keV) $= 20[1 - (r/a)^2]$, while the background beta is taken as, $\beta_{\mathrm{pc}} = 0.06[1 - (r/a)^2]$. If the system is unstable (i.e. $|\partial\beta_\alpha/\partial r| > |\partial\beta_{\alpha\mathrm{cr}}/\partial r|$), we assume that the TAE excitation will lead to radial diffusion of alpha particles with the transport described within the framework of a quasi-linear theory.

The basic quasi-linear model is presented in appendix B to which the reader can refer for more details. We shall assume that the unstable region lies within a single radial band. As we previously noted alpha particle transport is expected to flatten the alphas' beta profile beyond the unstable region of linear theory and a relaxed (denoted as 'rlx') alpha particle beta profile $\beta_{\alpha\mathrm{rlx}}(r)$ will form. To find the region to which that alpha particle spread to and $\beta_{\alpha\mathrm{rlx}}(r)$, we note that the quasi-linear theoretical model predicts that the original unstable region spreads in space to satisfy the condition $\partial\beta_{\alpha\mathrm{rlx}}/\partial r = \partial\beta_{\alpha\mathrm{cr}}/\partial r$ in a region $r_1 < r < r_3$, and at these interfaces $\beta_{\alpha\mathrm{rlx}}(r_{1,3}) = \beta_\alpha(r_{1,3})$. Our task is to find r_1 and r_3 in accord with the procedure described in appendix B. There, it is also shown that there will be a point r_2 between r_1 and r_3 that satisfies $\beta_{\alpha\mathrm{rlx}}(r_2) = \beta_\alpha(r_2)$. These previous assertions assume that r_1 and r_3 will be found to lie within the boundaries of the plasma. Now, the original beta profile, $\beta_\alpha(r)$, is determined by classical processes which balance fusion energy production with the alpha particle drag to the plasma. In the relaxed state the beta profile remains $\beta_\alpha(r)$ outside the relaxed region, while the beta profile is at marginal stability within the relaxed region. Hence within the relaxed region, we find $\beta_{\alpha\mathrm{rlx}}(r) = \beta_\alpha(r_1) + \int_{r_1}^{r}(\partial\beta_{\alpha\mathrm{cr}}/\partial r')\mathrm{d}r'$. As $\beta_{\alpha\mathrm{rlx}}(r_3) = \beta_\alpha(r_3)$, one of the conditions to determine the endpoints is, $\beta_\alpha(r_3) - \beta_\alpha(r_1) = \int_{r_1}^{r_3}(\partial\beta_{\alpha\mathrm{cr}}/\partial r')\mathrm{d}r'$. The additional condition is determined by the balance of classical processes with the quasi-linear diffusion of quasi-linear relaxation process in the TAE turbulent region. Appendix B indicates that applying a particle conservation condition in this region gives a reasonable estimate for this balance. Hence, the end-points of the turbulent region are determined by the additional condition $\int_{r_1}^{r_3}\beta_\alpha(r')r'\,\mathrm{d}r' = \int_{r_1}^{r_3}\beta_{\alpha\mathrm{rlx}}(r')r'\,\mathrm{d}r'$. Because our model omits the details of the velocity phase space redistribution, we note that the actual energy density that is redistributed is smaller than the above estimate [29]. Only a fraction, η, of the alpha particle beta profile undergoes redistribution due to the resonant interaction with TAE modes. In [29, 30] this fraction was estimated as $\eta = (v_{\alpha 0} - v_\parallel)v_\parallel/v_{\alpha 0}^2 \leqslant 0.25$ for the straight cylinder geometry, where $v_\parallel$ is the particle parallel velocity resonant with the TAE. As a result, in the relaxation region the beta profile can be expressed as $\hat{\beta}_\alpha(r) = \eta\beta_{\alpha\mathrm{rlx}}(r) + (1 - \eta)\beta_\alpha(r)$. Thus, the resulting alpha profile is given by

$$\hat{\beta}_\alpha(r) = \begin{cases} \beta_\alpha(r), & r < r_1, \\ \eta\beta_{\alpha\mathrm{rlx}}(r) + (1-\eta)\beta_\alpha(r), & r_1 < r < r_3, \\ \beta_\alpha(r), & r > r_3. \end{cases} \tag{12}$$

In figure 12 we show the result of the relaxation of the beta profile with $\eta = 0.25$. Also, to demonstrate the sensitivity to the critical beta (and thus to the damping rate model) we show in addition an alpha particle profile obtained for the critical beta from equation (11) multiplied by 0.7, which is denoted as $\hat{\beta}_{\alpha 1}$. For the latter case, the alphas are found to be redistributed up to the plasma edge with 4% losses. For figure 12 we note that the TAEs are locally unstable within $0.39 < r/a < 0.72$. After the quasi-linear transport model is applied the alphas are redistributed within $r_1/a = 0.30 < r/a < r_3/a = 0.89$ (see curve marked with $\hat{\beta}_\alpha$) in figure 12. After the redistribution the growth rate in our model equals the damping rate, and, by making use of the result of [8], is $\gamma_\alpha = -\gamma_{\mathrm{iL}} - \gamma_{\mathrm{ecoll}} = 4\%$ at the most unstable point, $r/a \simeq 0.6$. Here, we used $s = 0.3$,

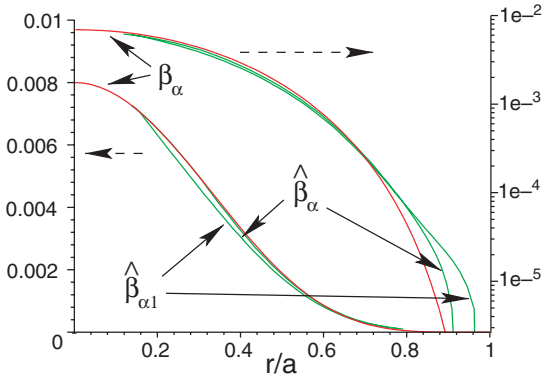

Figure 12. Alpha particle beta profiles initial and reconstructed using expressions for the local critical beta equation (11). Beta profile $\hat{\beta}_{\alpha 1}$ is obtained with the critical beta from equation (11) multiplied by 0.7. All the profiles are shown in linear and logarithmic scales.

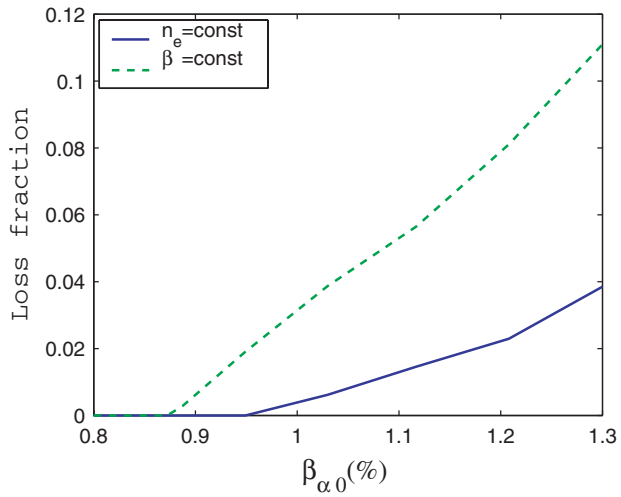

Figure 13. Expected alpha particle losses are shown as a function of increased $\beta_{\alpha 0}$ keeping the total plasma beta (- - -, $\beta \equiv \beta_{\rm pc} + \beta_\alpha = \text{const}$ in which $\beta_{\alpha 0} \sim T_{\rm i0}^{5/2}$) and density fixed (——, $\beta_{\alpha 0} \sim T_{\rm i0}^{7/2}$).

$q = 1.5$, $T_{\rm i} = 12\,\text{keV}$ ($T_{\rm i0} = 20\,\text{keV}$). This compares with the growth rate before the redistribution, $\gamma_\alpha \simeq 4.7\%$, for the same background plasma. Note that due to the global structure of the TAEs their growth/damping rates are typically much smaller than local theory predicts.

Stronger radial transport is expected if the thermal ion temperature is raised. This is because the fusion alpha-particle beta depends on $T_{\rm i}$: $\beta_\alpha/\beta_{\rm pc} = \sigma^2 0.117 T_{\rm i}^{5/2}/(1+\sigma)$, where $\sigma \equiv (n_{\rm D} + n_{\rm T})/n_{\rm e} = 0.8$. Figure 13 shows the expected loss dependence with increased alpha particle beta as the temperature was increased from a baseline case of $T_{\rm i0} = 20\,\text{keV}$, $\beta_{\rm pc0} = 6\%$ and $\beta_{\alpha 0} = 0.8\%$. Here, in one case, we fixed the plasma density (solid curve) and in another case, the plasma beta (dashed curve), while keeping fixed $r_3 = a$. In the case of fixed plasma density the predicted TAE induced transport is weaker because the ion Landau damping increases with ion temperature. With the constant beta, the ion temperature was varied from 20 keV at $\beta_{\alpha 0} = 0.8\%$ to ~24 keV at $\beta_{\alpha 0} = 1.3\%$, whereas at fixed density the corresponding temperature range was from 20 to ~23 keV. We see that losses can become severe with increased temperature especially for the fixed beta case (note that MHD considerations may limit the operational beta to a fixed value).

In the calculations in this section, we neglected the TAE interaction with beams assuming that only one specie is driving the instability. It should be possible to renormalize the critical gradients proportional to the contribution of each specie to the total drive. The model we propose needs to be corrected by numerical calculations to account for extra damping mechanisms. More detailed investigations can be adjusted to numerically evaluate damping and growth rates, as is obtained in NOVA-K. Our model shows that, in the case of local instability theory, the TAE instability effects allow the window of operation in ITER but will establish the high temperature limit. The quasi-linear theory applicability condition, which requires the overlap of particle resonances, must also be considered and this is a subject of further study.

7. Summary and discussion

We showed that NBI with tangential injection geometry is likely to destabilize TAEs in an ITER-like plasma. With perpendicular injection and/or lower beam energy one can reduce the TAE drive. Since the reactor plasma is supposed to be self-sustained without the beams, TAEs in an ITER-size machine will be driven only by alpha particles. As also follows from our previous study TAEs appear to be weakly unstable at operation where central temperatures are near 20 keV. On the other hand, NBI may provide an important tool for the experimental study of different types of AE instabilities by creating additional drive. Thus, it is important to plan the NBI to be as flexible as possible in order to be able to change the conditions of AE excitation, i.e. by changing the geometry angle, energy, specie etc.

A quasi-linear model for alpha particle TAE induced transport has been developed. A critical assumption for the applicability of this quasi-linear calculation is that the particle–TAE mode resonances are overlapped, an issue that needs further study. With this assumption of resonance overlap and assuming that spatially local conditions govern the growth of waves, a self-consistent set of equations have been obtained. The solution of these equations show that, just above marginal stability of the nonrelaxed slowing down distribution function, the instability region is localized to a small spatial region. The relaxation causes the unstable region to broaden so that the relaxed state has a β_α profile at marginal stability, over a broader spatial band, than the original instability band. If the global β_α is increased further (e.g. due to increased plasma temperature) beyond the marginal state, the relaxed spatial band of marginal instability increases further until the unstable band reaches the outer edge, where alpha particles are lost. The former case will not have a major effect on plasma performance. However, when alphas are lost to the edge, deleterious confinement conditions may then develop. For example, in our modelling we find that instability develops above 20 keV. However, direct alpha power losses to the wall greater than 5% (the standard that is often used to define deleterious conditions in ITER [31]) are predicted for a somewhat higher central plasma temperature (~23 keV).

More verification of this quasi-linear model is needed, but potentially it can be an important tool for predictive codes such as TRANSP to be used to evaluate the effects of TAE driven transport on reactor performance. In principle, one can determine the domain of plasma reactor parameters that can be achieved even with TAE unstable modes present.

Acknowledgments

Discussions with A. Polevoi have been valuable for ITER plasma modelling. This work was supported by the United States Department of Energy under Contracts No DE-AC02-76CH03073 and DE-FG03-96ER-54346.

Appendix A

In the case of a Lorentz collisional operator, $d_{\chi\chi} = 1 - \chi^2$, equation (1) transforms to the following

$$\frac{\partial \hat{f}}{\partial \tau} = \frac{\partial}{\partial \chi}(1-\chi^2)\frac{\partial \hat{f}}{\partial \chi} + Q\delta(\chi - \chi_0)\theta(\tau - \tau_0). \qquad (13)$$

Again, if the distribution function is narrow in pitch angles, we can first neglect the trapped/passing boundary and expand the solution in terms of the Legendre polynomials $P_l(\chi)$: $\hat{f} = \sum_l a_l(\tau)P_l(\chi)$. The solution at a given variable τ can be easily obtained:

$$\phi(\chi) = \sum_l a_{l0}\, \mathrm{e}^{-l(l+1)\tau} P_l(\chi), \qquad (14)$$

where $a_{l0} = (l+\frac{1}{2})\int_{-1}^{+1} P_l S(\chi-\chi_0)\mathrm{d}\chi$. Practically $0 \leqslant 1 \leqslant 26$ is required for good accuracy for the source term in the form $S = \mathrm{e}^{-(\chi-\chi_0)^2/\delta\chi^2}/\delta\chi\sqrt{\pi}$, and $\delta\chi = 0.1$. Pitch angle distribution accounting for the trapping region is obtained by substituting equation (14) into equation (7). Since this technique is not exact, the resulting distribution may have discontinuities if the width is large (or $\tau \geqslant \frac{1}{2}$). We propose a method that results in a good approximation to the exact solution. First, we account for the discontinuity by making the distribution continuous and renormalize it to conserve particles, which we denote by f'_χ. Second, we force it to become isotropic, $f_\chi = \frac{1}{2}$, at $\tau \to \infty$. Finally, the pitch angle part of the distribution function is given by

$$f_\chi = \frac{4\tau^3 + f'_\chi}{8\tau^3 + 1}, \qquad (15)$$

where parameters are adjusted for better agreement with the exact solution, which we find by performing Monte Carlo simulations. The comparison with the numerical simulation is shown in figure 14.

Appendix B

We seek a steady-state solution to a one-dimensional model we use to describe the energetic particle relaxation due to the TAE instability, where the density gradient causes the universal instability drive to be present. We use the model developed in [32]. This model considers the linear modes to be extremely localized, but continuously spread out in space. At each radial

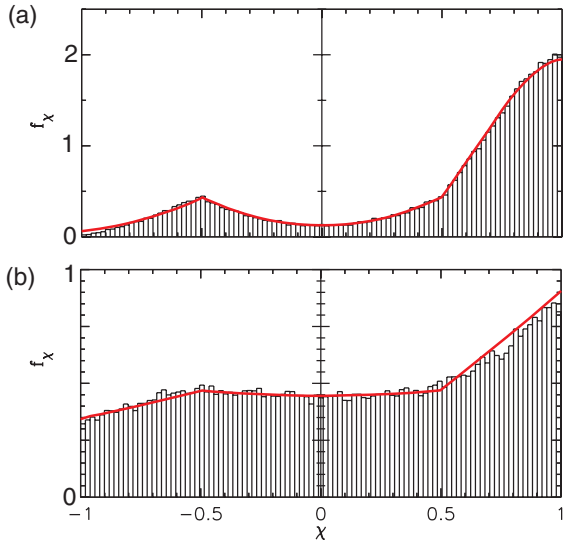

Figure 14. Comparison of the model pitch angle distribution function of beam ions, equation (15) (——) with the Monte Carlo simulation (shown as histograms) for the Lorentz scattering operator. (*a*) Corresponds to the distribution at $\tau = 0.09$ and (*b*) at $\tau = 0.4$.

point the diffusion coefficient D, which is proportional to the mean square value of the field amplitude, satisfies the evolution equation,

$$\frac{\partial D(x,t)}{\partial t} - 2[\gamma_\mathrm{L}(x,t) - \gamma_\mathrm{d}(x)]D(x,t) = 0, \qquad (16)$$

where γ_d is the damping rate of the mode due to background dissipation and γ_L is the instability drive of the wave proportional to the radial spatial gradient of the distribution function. In this simplified model, we take

$$\gamma_\mathrm{L}(x,t) = -\sigma\frac{\partial f(x,t)}{\partial x}, \qquad (17)$$

where f is the time averaged distribution function for the energetic particles, x a normalized radial variable and σ a positive constant. The distribution function satisfies the quasi-linear equation that results from the diffusion arising from the unstable spectrum and the relaxation of the energetic particles from classical processes. The classical relaxation is taken to satisfy a simple Krook collision operator with a relaxation rate ν and with a source present, which is of the form $\nu(x)f_0(x)$. The kinetic equation for the system is:

$$\frac{\partial f}{\partial t} - \frac{\partial}{\partial x}D(x)\frac{\partial f}{\partial x} = \nu(x)(f_0 - f). \qquad (18)$$

Clearly when $D = 0$, the steady solution is $f = f_0$, and this solution can be sustained when there is stability everywhere in space so that $\gamma_\mathrm{d} > \gamma_\mathrm{L} \equiv -\sigma\partial f_0/\partial x$.

Suppose now $\gamma_\mathrm{L} > \gamma_\mathrm{d}$ in a spatial interval $x^- < x < x^+$. In that case, the diffusion coefficient grows and attempts to flatten the distribution function in the unstable region. However, the flattening causes gradients to steepen at the interface between the original stable and unstable regions. As a result the unstable region broadens beyond the interval between x^- and x^+. The final distribution is expected to have the form of figure 15 where the relaxation band spreads

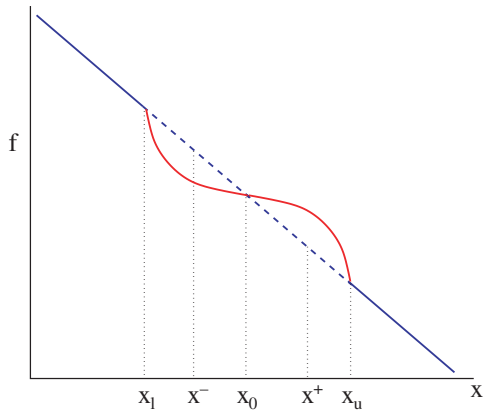

Figure 15. Relaxation of an initial equilibrium to the marginal stable one. Notation is explained in the text.

out to a larger interval. The region of relaxation stops only where the diffusion coefficient vanishes at the points x_u and x_l. The distribution will be continuous at the points x_u and x_l so that the shape of the $f_0(x_0)$ is such that we will have an intermediate point x_0 where $f(x_0) = f_0(x_0)$, as can be seen in figure 15.

We now solve equations (16)–(18) in the steady state to determine the final relaxed region. We can choose a suitable normalization that allows us to take $\sigma = 1$. In this case, we find as steady solutions

$$\frac{\partial f_0}{\partial x} = -\gamma_L, \qquad \frac{\partial f}{\partial x} = -\gamma_d \tag{19}$$

and the relation,

$$\frac{\partial D\gamma_d}{\partial x} = -\nu(x)\int_{x_0}^{x}[\gamma_L(x') - \gamma_d(x')]dx'. \tag{20}$$

Now, integrating equation (19) with the condition that $D(x)$ vanishes at the end points $x = x_l, x_u$, yields the relations

$$D(x)\gamma_d(x) = D(x_0)\gamma_d(x_0) - \int_{x_0}^{x}\nu(x') \times \int_{x_0}^{x'}[\gamma_L(x'') - \gamma_d(x'')]dx'', \tag{21}$$

$$D(x_0)\gamma_d(x_0) = \int_{x_0}^{x_u} dx'\nu(x')\int_{x_0}^{x'}[\gamma_L(x'') - \gamma_d(x'')]dx'', \tag{22}$$

$$\int_{x_l}^{x_u} dx\ \nu(x)\int_{x_0}^{x}[\gamma_L(x') - \gamma_d(x')]dx' = 0. \tag{23}$$

Note that equation (20) implies that $D(x)\gamma_d(x)$ is maximum at x_0, as at that point $\gamma_L(x_0) > \gamma_d(x_0)$. The points x_l, x_0 and x_u are determined from equation (23) and the two relations

$$\int_{x_0}^{x_{l,u}}[\gamma_L(x) - \gamma_d(x)]dx = 0. \tag{24}$$

This last equation follows from the equality of f and f_0 at $x = x_l, x_0$ and x_u and the x-integration of equations (19).

As an example, consider the case where f_0 has a constant slope so that γ_L is a constant and γ_d has the form $\gamma_d = \gamma_{d0}[1 + a(x - x_0')^2]$, with $\gamma_L > \gamma_{d0}$. The original unstable region is contained within the band $x^- < x < x^+$, where

$$x^{\pm} = x_0' \pm \left(\frac{\gamma_L - \gamma_{d0}}{a\gamma_{d0}}\right)^{1/2}. \tag{25}$$

The solutions for the end points x_l, x_0 and x_u are found from equations (23) and (24) to be, $x_{u,l} - x_0' = \pm(6((\gamma_L - \gamma_{d0})/a\gamma_{d0}))^{1/2}$, $x_0 = x_0'$. Thus, the unstable region is considerably broadened, but if this region is within the boundaries of the plasma, the diffusion does not lead to excessive energetic particle loss.

We observe that this theory gives a very simple method of estimating the energetic particle relaxation due to instability, and it is readily generalized to more complicated systems. In the text we take the radial coordinate as $x = r^2/2$, and apply this result to the expected $\gamma_L \sim \gamma_d$ that arises in linearized TAE theory.

There are several important points that are in need of further investigation that is pertinent in assessing the robustness of this procedure. One has to note that the physical problem is in more than one phase space dimension. As a result, even in the spatially unstable region, only a fraction of the particles that are slowing down in velocity space would have resonantly interacted with the wave and relaxed its distribution in the manner described in this theory. Kolesnichenko [29,30] has estimated that in a burning plasma the fraction, η, of relaxed particles in the unstable region is $\eta \sim 0.25$. Another important point is that the quasi-linear model that has been used is based on the assumption that the basic TAE modes cause resonant particle-mode overlap, so that the particles can diffuse stochastically in the unstable region. However, we see from equation (22), that the diffusion coefficient is proportional to the relatively weak classical relaxation rate ν. As a result, it is possible that the mode amplitudes of the finite number of TAE modes that is predicted to be excited in a steady-state solution are not large enough to achieve the mode overlap that is needed to justify the analysis. In this case, it has been pointed out in [32] that rather than a steady behaviour, bursty behaviour arises where the instantaneous mode amplitude, and hence diffusion, is much larger than that for the steady-state prediction. This is an important subtle issue that will be addressed in later work. Yet another issue is the effect of finite orbit size in a tokamak plasma and how it is enhanced by field ripple for alpha particles near the edge. This effect is particularly important if the unstable region is predicted to move out to near the plasma edge.

References

[1] Cheng C.Z., Chen L. and Chance M.S. 1985 *Ann. Phys. (NY)* **161** 21
[2] Cheng C.Z. and Chance M.S. 1986 *Phys. Fluids* **29** 3695
[3] Cheng C.Z., Fu G.Y. and Van Dam J.W. 1988 *Proc. Joint Varrena–Lausanne Workshop on Theory of Fusion Plasmas (Lausanne, Switzerland, 3–7 October 1988)* pp 259–70 *Princeton Plasma Physics Laboratory Report* PPPL-2585 (January, 1989) p 14
[4] Fu G.Y. and Van Dam J.W. 1989 *Phys. Fluids* B **1** 1949
[5] Wong K.L. 1999 *Plasma Phys. Control. Fusion* **41** R1
[6] Heidbrink W.W. and Sadler G.J. 1994 *Nucl. Fusion* **34** 535
[7] Campbell D.J. 2001 *Phys. Plasmas* **8** 2041
[8] Gorelenkov N.N. *et al* 2003 *Nucl. Fusion* **43** 594

[9] Cheng C.Z. 1992 *Phys. Rep.* **211** 1
[10] Gorelenkov N.N., Cheng C.Z. and Fu G.Y. 1999 *Phys. Plasmas* **6** 2802
[11] Fu G.Y., Nazikian R., Budny R.V. and Chang Z. 1998 *Phys. Plasmas* **5** 4284
[12] Nazikian R. *et al* 1997 *Phys. Rev. Lett.* **78** 2976
[13] Kramer G.J. *et al* 2004 *Phys. Rev. Lett.* **92** 015001-1
[14] Budny R.V. 2002 *Nucl. Fusion* **42** 1383
[15] Putvinskij S.V. 1986 *Reviews of Plasma Physics* vol 18, ed B.B. Kadomtsev (New York: Consultants Bureau) p 239
[16] Berk H.L., Horton W., Rosenbluth M.N. and Rutherford P.H. 1975 *Nucl. Fusion* **15** 819
[17] Angioni C. *et al* 2002 *Plasma Phys. Control. Fusion* **44** 205
[18] Bernabei S. *et al* 2001 *Nucl. Fusion* **41** 513
[19] Gorelenkov N.N. *et al* 2000 *Nucl. Fusion* **40** 1311
[20] Kramer G.J., Cheng C.Z., Fu G.Y., Kusama Y., Nazikian R., Ozeki T. and Tobita K. 1999 *Phys. Rev. Lett.* **83** 2961
[21] Berk H.L., Van Dam J.W., Guo Z. and Lindberg D.M. 1992 *Phys. Fluids* B **4** 1806
[22] Rosenbluth M.N., Berk H.L., Van Dam J.W. and Lindberg D.M. 1992 *Phys. Fluids* B **4** 2189
[23] Testa D. and Fasoli A. 2001 *Nucl. Fusion* **41** 809
[24] Snipes J. *et al* 2004 Active and fast particle driven Alfven eigenmodes in Alcator C-mod *Bull. Am. Phys. Soc.* **49** 248
Snipes J. *et al* 2005 *Phys. Plasmas* **12**
[25] Berk H.L., Breizman B.N. and Ye H. 1992 *Phys. Lett.* A **162** 475
[26] Gorelenkov N.N. 1992 *Sov. J. Plasma Phys.* **18** 289
[27] Gorelenkov N.N. 1993 *Plasma Phys. Rep.* **19** 404
[28] Li Y.M., Mahajan S.M. and Ross D.W. 1987 *Phys. Fluids* **30** 1466
[29] Kolesnichenko Ya.I. 1980 *Nucl. Fusion* **20** 727
[30] Belikov V.S., Kolesnichenko Ya.I. and Lutsenko V.V. 1995 *Nucl. Fusion* **35** 207
[31] Jacquinot J. *et al* 1999 *Nucl. Fusion* **39** 2471
[32] Berk H.L., Breizman B.N., Fitzpatrick J. and Wong H.V. 1995 *Nucl. Fusion* **35** 1661